*Physics – Uspekhi* **58** (4) 330 – 344 (2015) 

*REVIEWS OF TOPICAL PROBLEMS* PACS numbers: 61.05.F –, 61.66.Dk, **63.20.–e**

# High borides: determining the features and details of lattice dynamics from neutron spectroscopy

P A Alekseev

DOI: 10.3367/UFNe.0185.201504b.0353

## Contents



**Abstract.** **We review wide-ranging research that combines inelastic neutron scattering spectroscopy with phenomenological and *ab initio* calculations to study the lattice dynamics and specifics of the electron–phonon interaction in three-dimensional boron cluster network systems $MB_6$ and $MB_{12}$ ($M$ = La, Sm, and Yb, Lu, Zr). A close similarity is found between the atomic vibration spectra of these systems, which is fundamentally due to a strong hierarchy of interatomic interaction in these systems and which manifests itself both in the shape of the low-energy phonon dispersion and in the position of the high-energy edge of the spectrum. Manifestations of strong electron–phonon interactions in the lattice vibration spectra of borides are studied in detail and their relation to the nature and features of the valence-unstable state of rare-earth ions is examined. Resonance nonadiabaticity and magnetovibration interaction effects in spin- and valence-fluctuating systems are given special attention.**

**Keywords:** neutron spectroscopy, phonon spectra, electron–phonon interaction, rare-earth borides

## 1. Introduction

Elementary boron involved in the formation of different compounds demonstrates a tendency to create two-dimensional atomic structures or three-dimensional clusters, by analogy with carbon, a neighboring element in the periodic table. Carbon is intensively investigated, with new forms of its existence being discovered (nanotubes, fullerenes, graphene, and their derivatives). The considerable interest in borides is also quite obvious, being related to prominent (physical, chemical, and mechanical) properties of a large number of cluster framework and stratified structures. Examples are $MgB_2$ as a superconductor, $LaB_6$ as an electrophysical material with high emitting ability, and the narrow-band strongly correlated semiconductor $YbB_{12}$ [1].

The boron atom has one electron fewer than carbon; therefore, it appears to be electron-deficient in forming spatial structures analogical to carbon. As a result, boron clusters and stratified structures are bound well with metallic elements and especially with rare-earth (RE) trivalent ions. The electron deficiency results in the formation of 'economic' boron cluster structures from the standpoint of covalent bonding. Due to this, metallic ions are typically localized in the free space between or inside boron 'blocs' or 'clusters'. Extra electrons from metallic ions stabilize the substance and determine the electrical properties of the material. In the case of the formation of structures based on f-electron metals, RE ions appear to be a source of various unusual physical properties of the system and, accordingly, allows varying them. This is due to the deep spatial localization in an atom specific to the f-shell and, on the other hand, its quite low binding energy.

From the standpoint of applying such systems as functional materials, the covalently bonded boron cluster network provides stability and firmness of the substance to exposure (chemical, thermal, mechanical) and, on the other hand, the properties of metallic atoms incorporated into a cluster network provide tuning of the electronic, magnetic, and thermal properties. Boron has a strong affinity to rare-earth elements, and forms RE borides, which are of particular interest [2]. We note that such an unusual phenomenon as fluctuative or intermediate valence was discovered in the study of the properties of samarium hexaboride conducted by Soviet physicists [3].

Among the framework cluster systems based on RE metals, $REB_6$ and $REB_{12}$ systems are well known and extensively studied. A general view of the structure of such systems is presented in Fig. 1. It can be seen that the boron

**P A Alekseev** National Research Center 'Kurchatov Institute',
pl. Akademika Kurchatova 1, 123182 Moscow, Russian Federation;
National Research Nuclear University 'MEPhI',
Kashirskoe shosse 31, 115409 Moscow, Russian Federation
E-mail: pavel_alekseev-r@mail.ru

Received 16 July 2014, revised 24 September 2014
*Uspekhi Fizicheskikh Nauk* **185** (4) 353 – 370 (2015)
DOI: 10.3367/UFNr.0185.201504b.0353
Translated by P A Alekseev; edited by A M Semikhatov

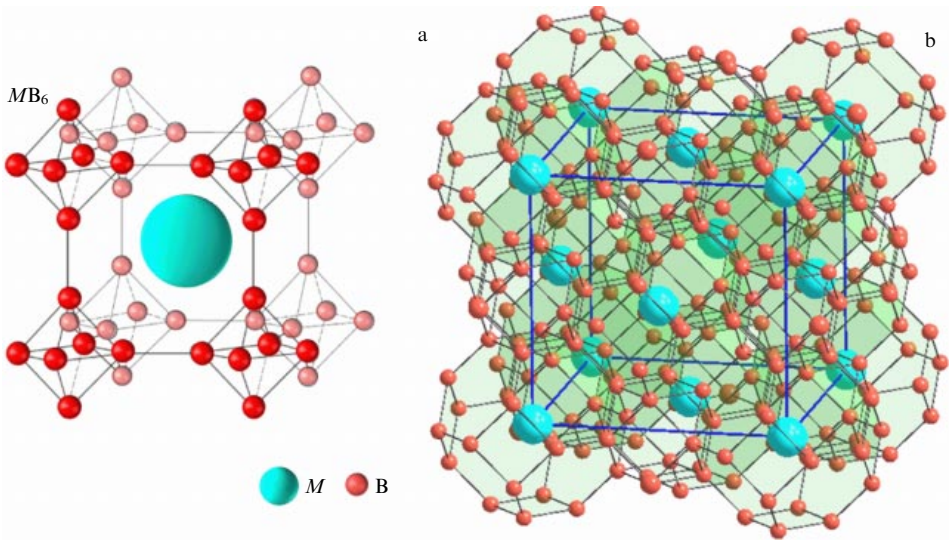


**Figure 1.** Cubic crystal structure of (a) $MB_6$ and (b) $MB_{12}$ compounds. The main parameters of the structures presented (lattice type and the lattice parameter $a$, space group, positions of RE ions ($M$) and boron (B)) are: (a) $CaB_6$ (CsCl), $a = 4.13$ Å, $Pm$-3$m$, $M(0,0,0)$, $B(1/2,\ 1/2,\ x)$, and $x = 0.20(1)$; (b) $UB_{12}$(NaCl), $a = 7.47$ Å, $Fm$-3$m$, $M(0,0,0)$, $B(1/2,\ x,\ x)$, and $x = 0.17(1)$.

framework is organized from boron clusters: $B_6$ octahedrons and $B_{12}$ dodecahedrons.

The $REB_6$ and $REB_{12}$ systems demonstrate the effects of strong electron correlations, superconductivity, and magnetic phase transitions in a variety of long-range magnetically ordered structures. By virtue of the peculiar structure, the considerable difference between the masses of boron and f- (d-) elements, and the formation of different types of ground states, it is reasonable to expect specific features in the spectra of elementary excitations of these systems, first and foremost in the spectra of the vibration density of states and in dispersion of phonons.

The lattice dynamics are usually strongly dependent on particular details of inter-atomic forces and on the interaction between structural elements that can form sublattices in a particular substance [4]. Consequently, features of the lattice dynamics reflect not only factors based on the formation of the crystalline structure for this class of materials but also all physically meaningful features of electron–phonon, magneto-vibrational interactions inherent to the physics of the compounds under consideration.

The first publications on the synthesis methods and properties of metal borides appeared in the 1960s (some of them were presented in [5]), and since then the question of the character of bonding in these systems has been of high interest. The discovery of the small electron gap formation on decreasing the temperature first in $SmB_6$ [6] and then in $YbB_{12}$ [7], treated as a manifestation of the metal–semiconductor transition in connection with f-electron instability, led to the increased interest in the physics of these systems, and, in particular, in the effects of electron–phonon interactions.

Early studies of lattice dynamics began in the 1970s. Several Raman-active modes were observed initially in the range 150 – 1400 $cm^{-1}$ (approximately 20–180 meV) [8, 9]. A systematic analysis of Raman data shows [10] that only one optical mode ($T_{1u}$) at the lowest measured phonon frequency has an opposite frequency dependence on the lattice spacing for a series of RE hexaborides, with respect to three others modes ($T_{2g}$, $E_g$, $A_{1g}$) observed in the range 650–1300 $cm^{-1}$, which expectedly increase its frequencies upon decreasing the lattice spacing. For $T_{1u}$ (whose frequency is approximately twice that of the acoustic phonon defined in neutron study [11]), the energy decrease on volume contraction can be an indication of an extra contribution to the Gruneisen parameters from the f-electron subsystem. Moreover, the particular softening of the $T_{1u}$ mode for $SmB_6$ with respect to the interpolation line from the other $REB_6$ substance was interpreted as the first evidence of the interplay of phonons with 'valence fluctuations'.

The first measurements of the phonon density of states for rich borides were done with $La^{11}B_6$ [12] and were compared with model calculations in [12, 13]. None of the three data sets reasonably corresponded with the others. Therefore, a number of questions connected with lattice dynamics had to be answered, to provide a better insight into the basic physics of borides, the background of their specific structure, and, in particular, those representatives of the class of strongly correlated electron systems. These questions can be formulated as follows.

— What are the energy structure of the phonon density of states in hexa- and dodecaborides, and the energy distribution of the partial contribution of the elements to the spectrum of atomic vibrations?

— How does the interplay between electronic and lattice vibration subsystems become apparent in the phonon spectrum?

A crucial and intriguing point was: what are the specific characteristics of the electron–phonon interaction for unstable valence and/or so-called Kondo semiconductors, which are represented by $SmB_6$ and $YbB_{12}$? In particular, could we obtain information on the origin and features of the initially (in the early 1980s) mysterious valence fluctuative ground state of some f-elements, apparently related to the phonon subsystem by charge fluctuations (as well as to magnetic excitations by spin fluctuations)?

These problems can be effectively studied by applying inelastic neutron scattering methods due to specific advantages of thermal neutrons as a probe for micro-dynamics.

Results and a discussion of the original and detailed research on lattice dynamics [dispersion curves of phonons

and spectra of the phonon density of states (PDOS)] are presented here for a number of $MB_6$ and $MB_{12}$ compounds obtained both by model calculations and experimentally, mainly by inelastic neutron scattering. The systems under study are primarily the strongly correlated electron systems like $SmB_6$ [14–16], $YbB_{12}$ [17–20], and $PrB_6$ [21] and their structural analogues $LaB_6$ and $LuB_{12}$, also including the $ZrB_{12}$ superconductor ($T_c = 6$ K) [22, 23].

Richer boron systems like higher borides $MB_{50}$, $MB_{66}$, three-component boron-based systems, etc., are not the subject of this paper. Reviews of their transport, thermodynamic, and structural properties can be found elsewhere (see [1]).

## 2. About the experimental methods

Inelastic thermal neutron scattering (with the energy transfer range $10^{-1}-10^{-3}$ eV) presently appears to be the most universal method for studying the lattice dynamics of materials. It was invented about 60 years ago and has been continuously improved. The competitive strength of the method is based on the number of peculiar properties of thermal neutrons important for application to condensed matter research. The most important of them are as follows.

— Charge neutrality, providing a high penetration ability of neutrons with respect to X-rays and charged particles.

— Energy and wavelength of thermal neutrons comparable with the excitation energy and inter-atomic distances in solids.

— Comparable amplitudes of nuclear and magnetic scattering (due to the magnetic moment of the neutron), which allow using the same instrument to study lattice and magnetic excitations. Nuclear scattering amplitudes are not systematically dependent on the nucleus charge. More details on this subject can be found in textbooks [24, 25]; we only remark that the above features ensure that the neutron scattering technique will be in demand for a long time into the future.

The two main types of neutron spectrometers, the three-axis spectrometer (TAS) and the time-of-flight spectrometer (TOFS), are usually considered as instruments that provide information on the dispersion of particular phonon modes and general spectral characteristics of the PDOS $g(\omega)$. Schematics of both instruments are shown in Fig. 2.

Basically, these two 'branches' of instrumentation arise from the dualism of the neutron as a quantum object: neutrons demonstrate properties of waves and particles. Therefore, the energy of a neutron can be determined from Bragg's law by diffraction on a crystal in the first case or measured by fixing, with the required accuracy, the time necessary for a neutron to fly from the source to the counter in the second one. Real examples of particular realizations of the above principles in instrumentation are presented in Fig. 3 and Fig. 4 (TAS and TOF spectrometers).

We briefly consider how the physical characteristics of phonons corresponding to collective atomic vibrations can be traced to real neutron spectra obtained from measurements using the instruments.

Equation (1) describes the relation between phonon dispersion modes and $g(\omega)$,

$$g(\omega)\,\mathrm{d}\omega = \frac{\Phi}{(2\pi)^3}\sum_{s=1}^{3r}\int \mathrm{d}C(\omega)\left|\mathrm{grad}_q\omega_s(q)\right|^{-1}. \qquad (1)$$

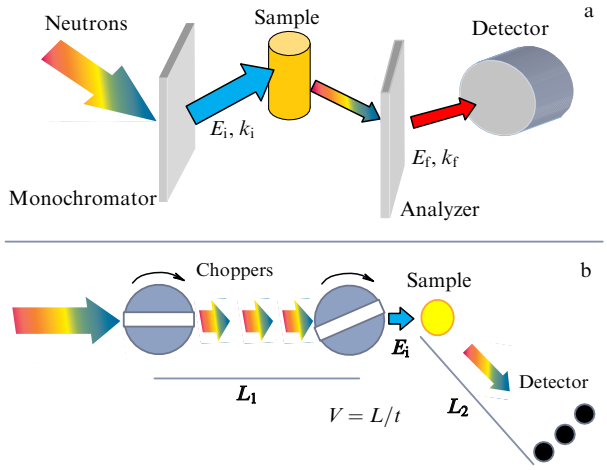


**Figure 2.** Schematics of (a) TAS and (b) TOFS spectrometers. (a) A polychromatic continuous neutron beam comes to the crystal monochromator, then a reflected monochromatic beam with an energy $E_i$ (wave-vector $k_i$) comes to the sample, where neutrons change their energy and wave vector (the latter is also defined by the scattering angle), a particular final the relevant energy $E_f$ and $k_f$ are selected by the crystal analyzer, and, finally, neutrons are counted by the detector. (b) A polychromatic continuous neutron beam comes to the two synchronized rotating choppers, producing neutron pulses with the incident energy $E_i$ selected due to the phase shift between choppers related to the flight pass $L_1$; the energy of scattered neutrons $E_f$ is determined by arrival time to the array of counters at the distance $L_2$.


**Figure 3.** Three-axis spectrometer IN20 at the Institut Laue–Langevin (ILL, Grenoble) [26]. *1* — monochromator shield, *2* — sample table with a goniometer and a sample in the cryostat, *3* — analyzer, and *4* — detector (each inside its shielding).

where $\mathrm{d}C(\omega)$ is an element of a constant-energy surface between the frequencies $\mathrm{d}\omega$.[1] The dispersion relation $\omega_s(q)$ is a particular $s$-phonon branch of $3r$ dispersion curves ($r$ is the total number of atoms in a primitive cell), and $\Phi$ is the volume of the crystal.

[1] Energy is defined as $E = \hbar\omega$, where $\omega$ is the frequency; in what follows, both notations are used in the sense of exchange by energy between neutrons and excitations (quasiparticles) in solids. The approximate relation between different units used in the spectroscopy of solids is 1 meV = 0.242 THz = 8 cm$^{-1}$.


**Figure 4.** MARI (multi angle rotor instrument) time-of-flight-spectrometer at the pulsed neutron source ISIS (Rutherford-Appleton Laboratory (RAL), Didcot) [27]. Here, the time structure of the neutron beam is provided (the mission of the first chopper in Fig. 2b) by the accelerator-based neutron source. *1* — background slow-chopper, *2* — Fermi-chopper for monochromatization, *3* — sample in the cryostat, *4* and *5* — detector array covering a scattering angle from 3° to 134° in the vertical plane.

The results of measurements with neutron spectrometers are typically presented in the form of the double differential cross section, which corresponds to the relative number of neutrons scattered into a solid angle element $\mathrm{d}\Omega$ within an energy transfer interval $\mathrm{d}\varepsilon$. It is determined by the scattering law $S(Q, E)$ that expresses the spectral characteristics of the substance under study with the transferred excitation energy $E = \hbar\omega$ and momentum $\mathbf{Q}$:

$$\frac{\mathrm{d}^2\sigma}{\mathrm{d}\Omega\,\mathrm{d}\varepsilon} = \frac{k}{k_0}\, S(\mathbf{Q}, \omega)\,,$$

where $k$ and $k_0$ are the final and initial neutron wave vectors in the scattering process. The corresponding formalism is considered in all necessary details in special literature [24, 28, 29]. In this paper, we discuss only a few specific features of the neutron scattering technique, which are important for an adequate and qualitative understanding of the results presented.

The first set of remarks concerns the specific features of instrumentation. The TAS spectrometer was initially designed to investigate details of dispersion curves of phonons (and also magnons) for single-crystal samples built from atoms with a dominant coherent amplitude of neutron scattering. This mission is realized by TAS due to its ability to determine momentum transfer vector components and energy transfer in a sufficiently large area of the momentum-transfer–energy space in a particular scattering plane with the necessary accuracy.

TOF spectrometers were oriented toward studies of PDOS spectra, initially operating with predominantly incoherent scattering materials [see Eqn (2)]. Later on, it was established that the use of a multidetector with a large scattering angle aperture including high scattering angles allows reaching the "incoherent approximation limit" even for a predominantly coherent scatterer by using the powder state of the sample. In fact, modern TOF spectrometers (see Fig. 4) allow obtaining a PDOS spectrum for any material in the powder state and some dispersion characteristics for coherent scatterers by the use of a single-crystal sample:

$$\frac{\mathrm{d}^2\sigma^{\pm}}{\mathrm{d}\Omega\,\mathrm{d}\omega_{\mathrm{inc}}} = \frac{k}{k_0}\, S(Q, \omega) = \frac{k}{k_0}\, b_{\mathrm{inc}}^2 \exp\left(-2W\right) \frac{Q^2}{6mN} \times g(\omega)\, \frac{1}{\omega}\, \frac{1}{\exp\left[\hbar\omega/(k_{\mathrm{B}}T)\right] - 1} \left\{ \begin{matrix} \exp\left(\dfrac{\hbar\omega}{k_{\mathrm{B}}T}\right) \\ 1 \end{matrix} \right\}. \quad (2)$$

Here, $\sigma^{\pm}$ corresponds to the scattering process with neutron energy loss (+) and neutron energy gain (−), $m$ is the atomic mass of the scatterer, $N$ is the number of particles, $T$ is the temperature of the sample, $b_{\mathrm{inc}}$ is the incoherent scattering amplitude, $W$ is the Debye–Waller factor, and $k_{\mathrm{B}}$ is the Boltzmann constant.

The second set of remarks concerns the specific relation between the dynamics of the crystal lattice and particular spectra obtained from neutron spectrometers. The main point is the 'mediator' between the neutron and the vibrating atom — the scattering amplitude that quantitatively determines the interaction between neutrons and atomic nuclei. Generally, it has two components: a coherent, $b_{\mathrm{c}}$, and an incoherent, $b_{\mathrm{inc}}$; the ratio between them is determined by the properties of the nucleus for a particular element on the level of its isotopes. The scattering amplitude has no systematic dependence on the atomic number of the element in the periodic table and can differ considerably, even for neighboring isotopes. Therefore, the scattering law $S(Q, E)$ measured with powder in a TOF experiment is directly proportional to the PDOS $g(E)$ only for single-element materials, as presented by Eqn (2). This $g(E)$ is just what is considered in calculations of physical properties such as heat capacity or the average vibration energy. In the case of a multi-element material, the relation between $g(E)$ and $S(Q, E)$ is not so straightforward.

For complex materials consisting of more than one element, $S(Q, E)$ measured in experiment is related to the so-called neutron weighted generalized PDOS $G(E)$:

$$\frac{\mathrm{d}^2\sigma^{\pm}}{\mathrm{d}\Omega\,\mathrm{d}\omega_{\mathrm{inc}}} = \frac{k}{k_0}\, S(Q, \omega) = \frac{k}{k_0}\, Q^2 G(\omega) \times \frac{1}{\omega}\, \frac{1}{\exp\left[\hbar\omega/(k_{\mathrm{B}}T)\right] - 1} \left\{ \begin{matrix} \exp\left(\dfrac{\hbar\omega}{k_{\mathrm{B}}T}\right) \\ 1 \end{matrix} \right\}, \quad (3)$$

where

$$G(\omega) = \sum_{\nu=1}^{P} c_\nu\, \frac{b_{\mathrm{inc},\,\nu}^2}{m_\nu}\, g_\nu(\omega)\,. \quad (4)$$

Here, $P$ is the number of different sorts of atoms with the scattering amplitude $b_\nu$, concentration $c_\nu$, and mass $m_\nu$, and the function $g_\nu(\omega)$ is a partial PDOS (see below):

$$g_\nu(\omega) = g(\omega) \exp\left(-2W_\nu\right) \left|\mathbf{e}_\nu(\omega)\right|^2. \quad (5)$$

Relations (3) and (4) are applicable to most presently studied materials with a multi-component structure. $G(E)$ contains the most general information on the structure and other characteristics of the lattice vibration spectrum and is determined by the partial density of the $g_\nu(E)$ states (related only to the particular $\nu$-sort of atoms in the substance; see Eqn (4)), which represent the contribution of every $\nu$-sort atom to $g_\nu(E)$ as defined by Eqn (5). Thus, the contribution of

each $g_\nu(E)$ to the scattering function $S(Q, E)$ is scaled by a particular ratio of the neutron scattering amplitude to the mass $m_\nu$ for every sort of atom.

The correspondence between the partial $g_\nu(E)$ and the total $g(E)$ is defined by the square of polarization vectors $|\mathbf{e}_\nu(\omega)|^2 \sim \sum_s |\mathbf{e}_{\nu,s}(\omega)|^2$ [in Eqn (5)] for $\nu$-sort atoms at a particular energy $E = \hbar\omega$ for all phonon branches (numbered by $s$) contributing to the physical density of states $g(E)$.

It is obvious that when $\nu > 1$, experiment does not directly provide $g(E)$, which is only physically meaningful from the thermodynamic standpoint. To obtain it, we need to make a model assumption on polarization vectors or to conduct more experiments with isostructural samples differing only by the scattering amplitude $b_\nu$. This possibility may be realized for elements that have isotopes with a large difference in the values of $b_\nu$. The corresponding method, named the isotopic contrast method, was developed in [30, 31]; it allows extracting the partial density of states $g_\nu(E)$ from experimentally obtained spectra after analyzing $P$ sets of measurements with samples that differ from one another by the $b_\nu$ composition. These approaches were successfully realized for HTSC materials [32, 33] and quasicrystals [34, 35].

The last remark is connected with neutron absorption. A system based on a number of natural elements like samarium, gadolinium, cadmium, boron, or some others cannot be studied by inelastic neutron scattering due to the very high absorption cross section. In fact, a layer consisting of such materials $\sim 0.1$ mm or less in thickness results in more than an order-of-magnitude attenuation of the thermal neutron beam. Therefore, the enrichment by low-absorption isotopes (such as $^{154}$Sm or $^{11}$B) to a high enough extent (typically not less than 99%) provides the only possibility of making spectroscopic measurements with reasonable statistical accuracy due to the increase in the sample volume available for scattering.

## 3. General remarks about the structure of phonon spectrums

Measured by the TOF method, the spectra $S(Q, E)$ for hexa- and dodecaborides [36, 37] (see Fig. 5 for $SmB_6$ and Fig. 6 for $YbB_{12}$) show that the boundary energy of phonons lies in the range 130–160 meV (the higher value corresponds to $MB_6$),

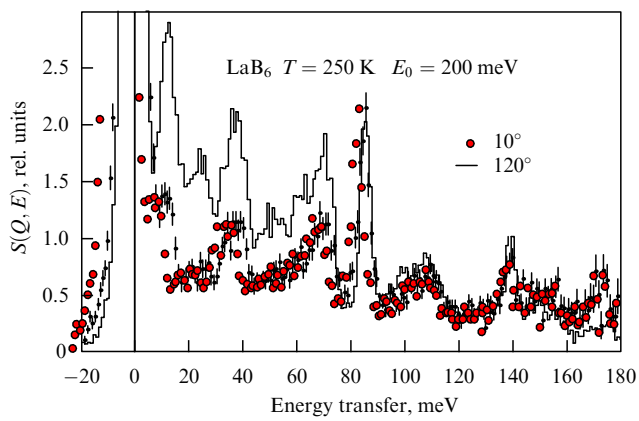


**Figure 5.** $S(Q, E)$ spectra for $LaB_6$ measured at temperature 250 K with initial energy $E_0 = 200$ meV on TOF spectrometer HET at ISIS at low (10°) and high (120°) scattering angle with resolution (FWHM) of 4 meV and 6 meV at zero energy transfer, respectively [36].

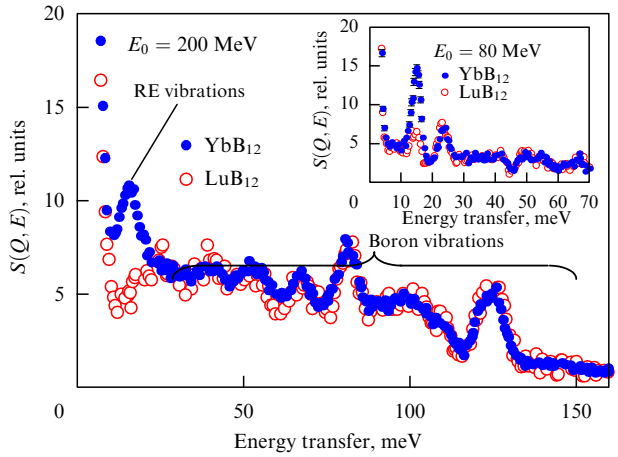


**Figure 6.** $S(Q, E)$ spectra for $LuB_{12}$ (light dots) and $YbB_{12}$ (dark dots) [37] measured at HET (ISIS) with $E_0 = 200$ meV at $T = 15$ K and high scattering angle (133°) corresponding to conditions for only the phonon contribution to the scattering function. Inset: spectra measured with $E_0 = 80$ meV (better resolution with respect to $E_0 = 200$ meV) and at $T = 160$ K.

i.e., in the range of relatively high energies in comparison with the spectra of traditional inorganic compounds. Measurements with such different RE elements as $M$ in $MB_n$ allow a practical realization of the method of 'isotopic contrast', due to the considerable difference in neutron scattering cross sections, for example, between Yb and Lu (more than by a factor of three). These nearby elements in the 4f-series have a small mass difference of the order of 1%. Owing to this type of experiment, the partial $g_M(\omega)$ and $g_B(\omega)$ have been determined [19]. It turned out that the thermal oscillation of heavy $M$-atoms is mainly concentrated in the range of energies below 20 meV, actually giving rise to the lowest energy peak of the DOS. Vibrations at higher frequencies are mainly related to boron motion, including clusters as structural units and their deformations of different symmetry types ('breathing', 'torsion', etc.).

From the standpoint of analysis and generalization, it is interesting to compare the boron DOS in intermetallic compounds with the DOS of pure boron and its analogue, graphite. In Fig. 7, the corresponding data from Raman-spectroscopy experiments are shown for elementary boron [38]. In the low-energy range, the strongest discrepancy is observed between experiment and simple model calculations for elementary boron [39]. The results of neutron spectroscopy studies of phonon spectra for carbon in two forms — graphite and single-wall carbon nanontubes — are shown in Fig. 8 (from original study [40]).

We note that the PDOS for graphite, graphite nanotubes, or cluster network substance $C_{60}$ (for the last, see, e.g., [42]) has the boundary energy at about 200 meV. These materials substantially differ from one another only in the energy range below 50 meV [40, 43] (see Fig. 8). For instance, libration modes have been observed at an energy of the order of a few meV for fullerene crystals [43].

It is seen from a comparison of Fig. 7 with Fig. 5 and Fig. 6 that the boundary energy for elementary boron is in the same range as for $REB_6$ and $REB_{12}$. The difference in phonon spectra is conspicuous for the low-energy part because of RE contributions to the DOS (direct as well as indirect). This quantitative difference and qualitative similarity between

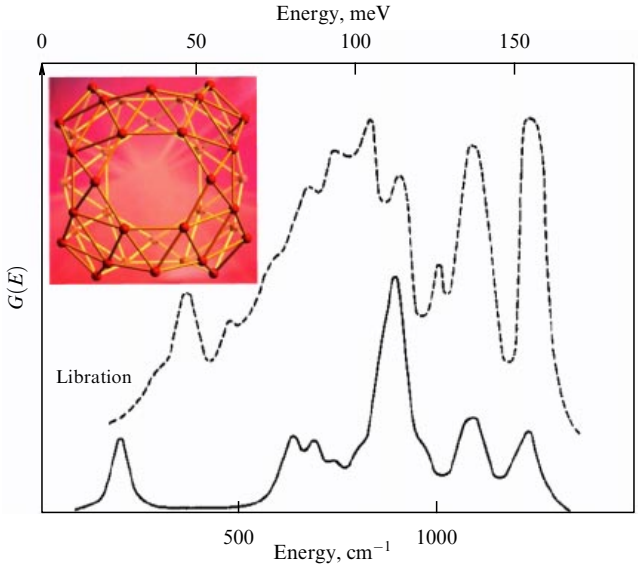


**Figure 7.** Comparison of the calculated PDOS (solid line) [39] and experimental results (dashed line) [38] obtained by the first-order Raman-spectroscopy study (hence, there is no indication of the acoustic mode) of elemental boron. Inset presents the design of the $B_{40}$ structure discovered in [41].

PDOS spectra of elemental boron and $MB_6$, as well as $MB_{12}$, is evidence that both (boron- and carbon-based) materials have a basic similarity in the type of bonding and the character of inter-atom interactions. Modification of the structure is mainly reflected by the low-energy PDOS for both (carbon- and boron-based) materials. The difference between them, as mentioned in the Introduction, is based on the number of effective electron covalent bonds and the resulting topological segregation and relative hardening of carbon–carbon bonding, which appears as an increase in the PDOS boundary energy by several dozen meV. The observed difference between phonon spectra of boron and carbon, regarded from the standpoint of the difference in the inter-atomic bonding, is related to the more explicit disposition of carbon to form 2D- and 3D-cluster frameworks, which is

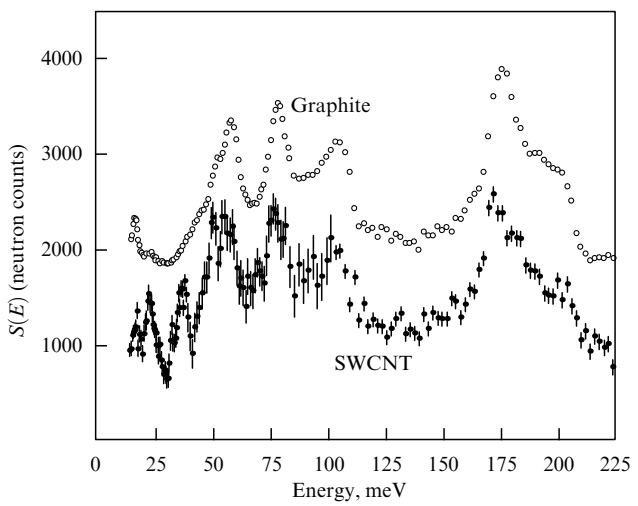


**Figure 8.** Comparison of the experimentally measured scattering function representing the PDOS of graphite (light dots) and SWCNT (dark dots) [40]. An essential difference is observed at excitation energies below 50 meV.

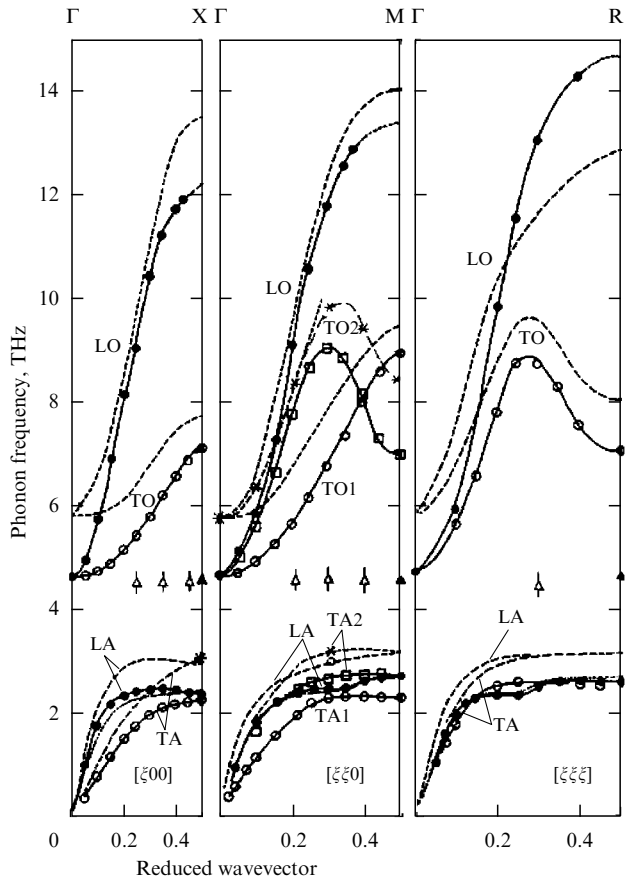


**Figure 9.** Phonon dispersion for SmB6 at room temperature, double isotopic single-crystal measurements at ATOS (IR-8, KIAE) and IN8 (ILL) [14]. Light dots and squares correspond to transverse acoustic (TA) and optical (TO) modes with polarization in the plane (100)–(011) (1) and perpendicular to it (2). Dark dots correspond to longitudinal (LA, LO) phonon modes. Triangles denote the dispersionless unpolarized mode in the region between the optical and acoustic bands (see Section 4). Dashed lines and stars show the data for the $La^{11}B_6$ single-crystal for different measurements starting from [11, 14]. The reduced wave vector is normalized to reciprocal lattice units for each direction.

easily demonstrated for boron only in the case of compositions with metals. Just recently, the first experimental evidence appeared [41] of the formation of some kind of buckyball structure (see the inset in Fig. 7) for pure boron: an all-boron fullerene-like cage cluster $B_{40}$ with an extremely low electron binding energy.

The first neutron experiments performed with single crystals of $MB_6$ ($LaB_6$ [44] and $SmB_6$ [14–16]) show a quite unusual picture of phonon dispersion in the range of relatively low phonon energies (below 15 meV). The dispersion curves of acoustic phonons exhibit quite extended flat parts (starting from $q/q_{max} \sim 0.25$ and continuing to the zone boundary) in all the main symmetry directions (see Fig. 9). The optical phonon band is typically separated from the acoustic branch by an energy gap of about 5 meV. The flat part of the acoustic dispersion curve can qualitatively be explained by the presence of a strongly expressed hierarchy of inter-ion interactions, primarily by RE atoms loosely coupled to one another, as well as a fairly weak connection between RE atoms and boric clusters. We note that in some cases, the energy band of flat acoustic phonon curves coincides with the energy range of magnetic excitations resulting from the f-electron spectrum.

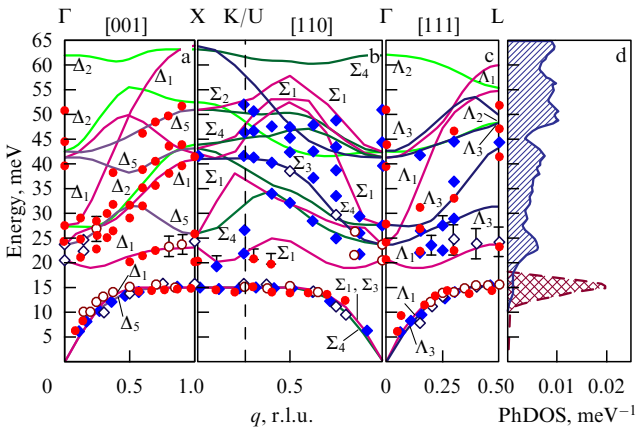


**Figure 10.** (a)–(c) Phonon dispersion curves for $YbB_{12}$ (light symbols) and $LuB_{12}$ (dark symbols) [45]. Circles: longitudinal branches; diamonds: transverse branches. The results of the model calculation are shown as solid lines [18]. Symmetries of phonons are labeled according to the Bouckaert–Smoluchowski–Wigner notation; $q$ is the reduced wave vector. (d) Calculated PDOS in $YbB_{12}$. Hatched area: boron partial PDOS, crossed-hatched pattern: ytterbium partial PDOS.

A similar/identical picture was obtained later in studies of $LuB_{12}$, $YbB_{12}$ [17–19, 45], and other $MB_{12}$ single crystals. In this connection, we note that estimations allow relating the volume of the 'void' in the center of the boric dodecahedron $B_{24}$ (in the $MB_{12}$ system) to the volume of RE ions localized in this space to be about 2/1, providing much free space for RE ions. Phenomenological calculations based on the forced-constant model (UNISOFT software package [46]) allowed obtaining a quite good description (see Fig. 10) of all available information (with 9 coordination spheres taken into account in [17, 18, 44]) on dispersion curves in the energy range up to 50 meV[2]. A strong hierarchy of interactions follows from model calculations, $\mathrm{RE-RE} \ll \mathrm{RE-B} \ll \mathrm{B-B}$, with a difference of approximately an order of magnitude at each stage. On the basis of this model and corresponding phenomenological parameters, the generalized density of states was calculated and compared with the one extracted from experimental data. A quite good description of the PDOS for acoustic and lower optical ranges (up to 40 meV) was obtained, but vibrations with higher energies (mainly pure boron) are not described, even at the qualitative level, and the only success of the above calculation in this energy range is the good correspondence between calculated and experimentally determined boundary energies of the phonon spectrum (see Fig. 11).

The phonon spectrums for $MB_{12}$ ($M$ = Lu, Yb, and Zr [23]) have been used to analyze the results of *ab initio* calculations (DFT–LDA). It appears that in the range of boron frequencies (Fig. 11), this type of calculation actually gives a quantitative coincidence with experiment, contrary to the phenomenological model [22, 19, 45]. But for phonon energies below 30 meV, the problems are aggravated. In particular, the calculation correctly provides the position of the first peak in the DOS but barely describes the peak at 25 meV. These features can be analyzed in more detail in investigations of single-crystal data using phonon dispersion (see below). Here, we simply mention that phenomenological approaches based on the Born–von Karmann approximation for a forced constant such as the UNISOFT package show that it is at least possible to elaborate an adequate enough model to describe phonons in the range of low-energy vibrations. On the other hand, the f- and d-electron influence is not described correctly in the pseudo-potential approach (such as DFT–LDA).

## 4. Electron–phonon interaction

There are several aspects of the electron–phonon interaction that are interesting to discuss for RE-based reach borides appearing as a three-dimension framework of boron clusters with incorporated positive-charge metallic ions.

1. Contribution of f-electrons to the bonding formation in this nanocluster base substance;

2. Effects of strong electron correlation in the sense of f–c hybridization:

2.1 Effects in lattice dynamics related to the phenomenon of a homogeneous mixed valence (intermediate valence) state of RE ions and charge fluctuations corresponding to this phenomenon;

2.2 Possible interaction between f-electron excitations (which define the magnetic excitation spectrum and conse-

[2] This value is limited by the typical energy range of TAS operating on thermal neutron beams.

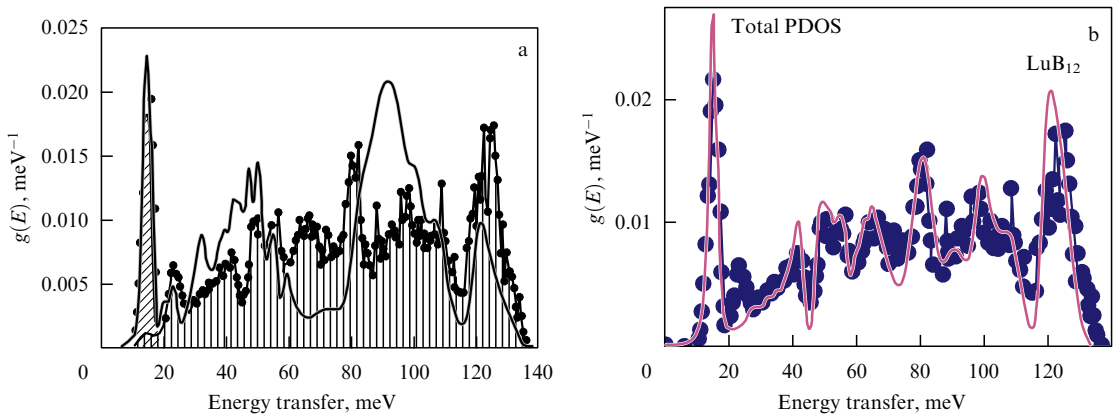


**Figure 11.** Experimentally defined [19] phonon density of states (PDOS) for $REB_{12}$ (dots). (a) Hatched area: boron partial PDOS, crossed-hatched pattern: ytterbium partial PDOS, solid line: a UNISOFT calculation of the PDOS converted with a resolution function for a TOF instrument. (b) The same experimental results for $LuB_{12}$ in comparison with DFT–LDA first-principle *ab initio* calculations [23] (solid line).

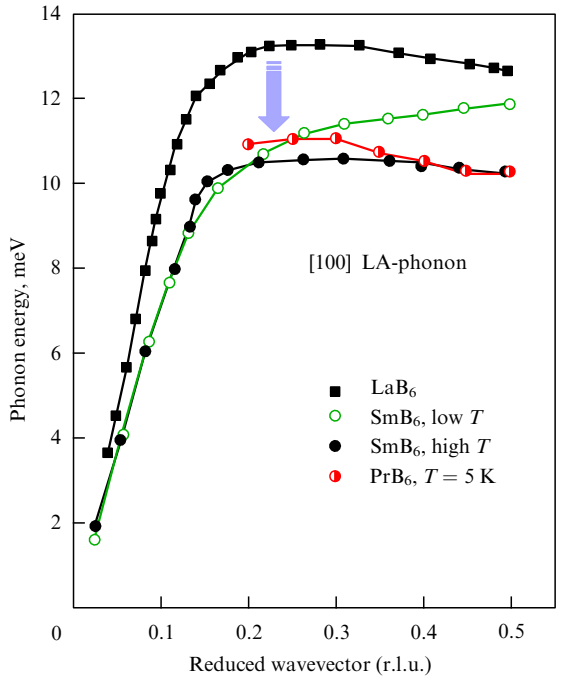


**Figure 12.** Longitudinal acoustic phonons from a single-crystal study of $REB_6$ systems. No temperature effects (between 300 K and 2 K) were observed in the dispersion (limited by the error bar of the size of the symbol) for $LaB_6$ or for $PrB_6$ (temperature in the range 2–50 K). ($SmB_6$ data are taken from [14–16].)

quently the dynamical magnetic susceptibility) and lattice vibrations, which could even be related to the formation of a specific ground state for the systems under study.

A systematic single-crystal study of phonon dispersion has shown that the presence of f-electrons in an RE ion at least substantially affects the energy of the flat part of acoustic branches. From the experimental data obtained by TAS measurements for single-crystal samples of hexaborides ($LaB_6$, $PrB_6$, and $SmB_6$; see Fig. 12), it appears that $PrB_6$ and $SmB_6$ demonstrate a coincidence of energies for the flat part [3] at the level of 10.5 meV within an experimental accuracy better than 0.1 meV, while for $LaB_6$, the same dispersion curve corresponds to the limit energy 13 meV.

The renormalization observed (indicated by the arrow in Fig. 12) cannot be the effect of mass difference between RE ions, because this factor is several times greater for the pair La–Sm than for La–Pr and, in any case, it is about 1%. Nor can this be the result of only a different number of f-electrons in the atomic shell of the $RE^{3+}$ ion or different values of the lattice spacing. The large difference that distinguishes an La-based substance from the other two is the valence band character: it is more d-type than f-type, as in Pr and Sm.

It is quite possible that the true reason for the observed effect is the hybridization nature of the formation of this large flat part of acoustic phonon modes, where the size of the gap between the modes of one symmetry type (one acoustic and one a low-lying optical one) is determined by an interplay of inter-atomic interactions between RE and B atoms, which is influenced by the energy structure and character of the electron subsystem. The atomic mass is then not the only or even a decisive factor for determining the energy of the corresponding mode, in spite of the resemblance of its origin to the so-called Einstein oscillator. Another interesting fact is that the experimental data available for the $ReB_{12}$ substance ($LuB_{12}-YbB_{12}$) does not show any evidence of the above-mentioned behavior of frequencies for acoustic phonons (cf. with Fig. 10).

In Sections 4.1 and 4.2, we detail the features of the manifestation of the electron–phonon interaction in the $REB_6$ and $MB_{12}$ systems, related to the effects of strong electron correlations; in other words, we discuss how the effect of interactions between localized and band electrons, in particular, of the valence (f-electron) instability and the formation of a Kondo-insulator-type ground state, manifests itself in the lattice dynamics.

### 4.1 $REB_6$

The $SmB_6$ system is actually the first compound with an anomalous lattice and electron properties that are related to the f-electron instability [3], giving rise to a large class of valence-unstable or intermediate-valence (intervalence) (IV) systems [47]. Striking representatives of this class of substance are metallic cerium ($\alpha-\gamma$ transition) and the compound SmS ('black' to 'gold' phase transition). For these systems, an external pressure less than 1 GPa results in the transformation to the IV state, accompanied by 'lattice collapse', resulting in a decrease in the volume by more than 10%. Recently, the first example of the same type of behavior was found for a 5f-electron material: the record volume collapse by 25% was observed for metallic plutonium ($\delta-\alpha$ Pu transformation) under the external pressure of only 0.2 GPa [48].

One of specific features of IV systems is the presence of inter-configuration, or charge fluctuations with the characteristic time scale $10^{-12}-10^{-14}$ s, which correspond by the order of magnitude to the frequency range of phonons in solids. It is clear that this 'resonance' condition allows expecting anomalies in the lattice dynamics resulting from the electron–phonon interaction. It can be primarily observed in longitudinal vibration modes, supposed to be the most sensitive to inter-atomic distance/charge modulations. In a search for and study of these effects, a number of especially targeted experiments were done in the 1980s and 1990s. A single-crystal study of lattice dynamics for 'classic' IV systems such as Sm(Y)S, SmS [49, 50], and $SmB_6$ [14, 15] was carried out on three-axis spectrometers. These experiments are substantially complicated by the necessity to use isotopically enriched materials ($^{154}$Sm nd $^{11}$B).

Measurements with the SmS system were done in [49, 50] at HFIR of the Oak Ridge National Laboratory in the early 1980s. Experiments on TAS instruments deal mainly with single-crystal samples, where part of the Sm was substituted by Y, which provided a 'chemical' compression effect (due to the difference in atomic volumes between Sm and Y) to obtain the IV state without applying external pressure, because a pressure above 0.6 GPa is needed for the transformation of pure SmS into the IV state.

Nevertheless, one of the successful TAS experiments was done [50] on a single crystal of SmS under a corresponding external pressure (at room temperature), allowing the observation of a dispersion of acoustic modes along the [111] direction. A kink-type anomaly was clearly observed in the longitudinal branch under pressure, which was attributed

[3] The dispersions for acoustic longitudinal phonons for $PrB_6$ are similar to those of $SmB_6$ in all symmetry directions except one important detail (see below): the absence of 'kinks' observed at $q/q_{max} \sim 0.3$ for $SmB_6$ along [110] and [111] (see Fig. 9).

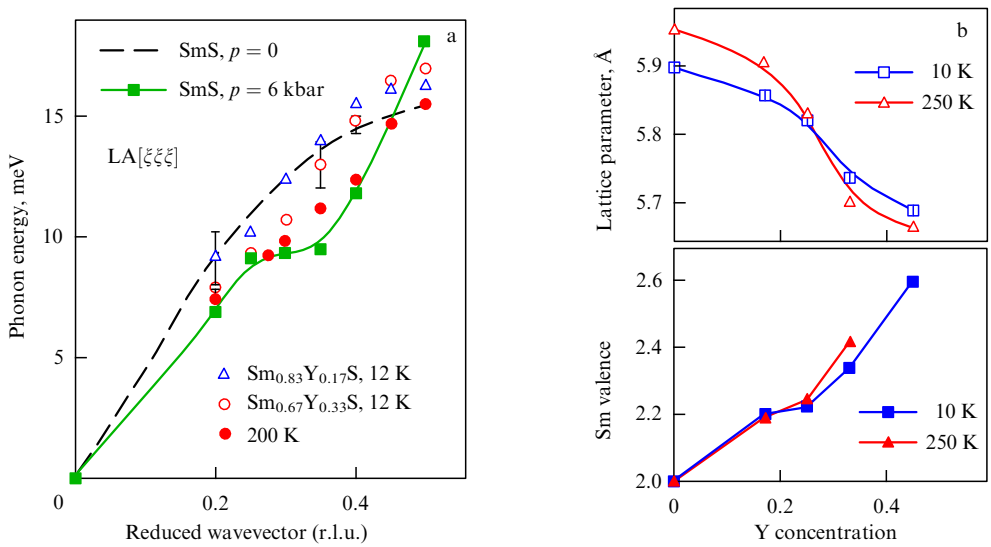


**Figure 13.** Left panel: dispersion curves of a longitudinal acoustic phonon in the [111] direction for SmS at $p = 0$ and $p = 0.6$ Pa [50] and for $Sm_{1-x}Y_xS$ [51] at $p = 0$. Right panel: Sm valence from L3-edge spectroscopy and lattice parameters from X-ray diffraction as a function of the yttrium concentration $x$ for two temperatures: 10 K and 250 K.

to the transition of the Sm ion to the IV state. The same effect has been detected for 'chemically' pressed $Sm_{1-x}Y_xS$ [49, 51] in the IV state (see Fig. 13) determined by L3-edge spectroscopy and lattice parameter measurements as a function of the Y-concentration $x$. It is clearly seen that the temperature affects the valence state of Sm and thus provides a modification of the 'kink' in the dispersion curves.

It should be mentioned that extra dispersionless vibration modes (with respect to 'normal' phonons expected for an NaCl-type structure for sulfides) have been fixed in the gap between optical and acoustic branches for the Sm(Y)S IV material [49]; similar ones were later clearly observed in experiments [14] with $SmB_6$ (see Fig. 9). In a pure-SmS high-pressure study [50], there was no indication of this mode, probably due to the limited range of experimental conditions available in the study. The dispersionless gap mode was initially attributed in [49] to so-called local vibrations due to substitution of a part of Sm atoms by Y atoms (the Y mass is about half that of Sm). This suggestion contradicts subsequent studies of the parameters of this mode as a function of temperature and the substituting element M for substances with different substitutions for Sm in the IV phase of Sm($M$)S. Finally, the extra 'gap mode' was identified as a specific feature (see below) resulting from the IV state of Sm [52, 53] in the systems under consideration.

The single-crystal of $SmB_6$ was investigated in the late 1980s–early 1990s using three-axis spectrometers of the IR-8 reactor at the RRC 'Kurchatov Institute', and then in more detail at ILL (Grenoble) [14, 15, 53]. The relevant compound, unlike SmS and metallic Ce, exists in the IV state (valence $\approx 2.55$) at ambient conditions; moreover, its valence temperature dependence is quite weak. The initial experiments with $SmB_6$ single crystals at room temperature demonstrated a number of anomalies in 'ordinary' phonon branches in comparison with the structural analogue $LaB_6$ (see Fig. 9): common softening of the acoustic and low optical branches and also 'kinks' at intermediate wave vectors (at about $q/q_{max} = 0.3$) on longitudinal acoustic branches along directions [110] and [111]. These anomalies have not been observed for the structure analogue $LaB_6$.

A microscopic analysis of the nature and properties of the features observed in the lattice dynamics of $SmB_6$ was successfully developed by Kikoin and Mishchenko [54] as a generalization of the previous study of the lattice dynamics of SmS [55, 56] based on the excitonic model of the intermediate valence state of the Sm ion suggested initially by Stevence [57]. The basic idea of the model is that in every Sm ion, the f-electron instability results in the formation of a quantum-mechanically mixed wave function

$$\tilde{f}_m = \{f^5_{J=5/2}\, f^*_{J=5/2}\}_m = f^6_m + f^5_m\, B^{(f)}_m\,. \qquad (6)$$

Thus, in each Sm ion, there is a superposition of two states of $f^6$ and $f^5B^{(f)}$, as shown by Eqn (6), which describe the two possibilities for localization of the loosely bound 6th $f^*$-electron (see Fig. 14). This electron either can occupy a place in the f-shell (that is, the configuration $f^6$ of $Sm^{2+}$,

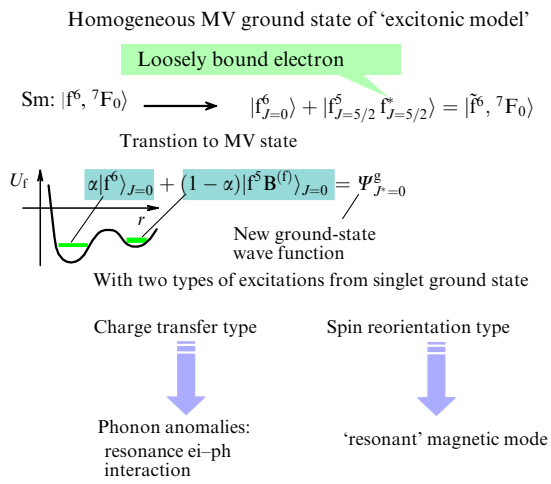


**Figure 14.** Representation of the mixed wave function of Sm in the intermediate valence state according to the model of an exciton of intermediate radius developed in [54] with the resulting two sets of excitation from the ground state.

which corresponds to the location of the 6th electron in the first well in the electron potential $U_f$ shown in Fig. 14) or, with some probability, 'leaves' for the orbitals of nearest neighbors, holding this distance due to the Coulomb interaction with a 'hole' appearing in the f-shell. In other words, it forms an excitonic-like state of intermediate radius, denoted as $f^5\,B^{(f)}$ and corresponding to the second well in Fig. 14.

The symmetry of this combined wave function describing a new IV state corresponds to the symmetry of the ground state of the $f^6$ multiplet due to a combination of the quantum numbers of the two interacting states in braces in Eqn (6). This feature gives rise to the main properties of the excitation spectrum connected with this new ground state of the f-shell formed as a singlet $^7F_0$.

Obviously, the spectrum of mixed wave function (6) can contain two different types or sets of excited states [58], as is schematically presented in Fig. 14. One set (spin-reorientation type) corresponds to the different mutual orientation of spin and orbital moments, forming the total $J = L + S$ of the complete wave function, but without a change in the charge density distribution, i.e., without a change in the probability of finding the 6th f-electron in one state or another in the right-hand side of Eqn (6) associated with two wells of the Sm atomic potential. This is the so-called 'magnetic' excitation, directly observed by means of dipole ($\Delta J = \pm 1$) intermultiplet spin–orbit-like transitions in the spectrum of neutron magnetic scattering. These excitations have been observed for $SmB_6$ [57, 59] and SmYS [51, 60, 61] in experiments using TAS and TOF spectrometers; the corresponding discussion is beyond the scope of this paper, being related to the ideas of 'resonant mode' formation in mixed-valence semiconductors [62].

Another (charge-transfer) type of excitations shown in Fig. 14 is related to states differing from the ground state by the probability of finding an f*-electron in one of two partial configurations in (6); the second type of excitation is connected to states with different characters of the charge density distribution. Such excitations can be regarded just as valence ('charge') fluctuations, but they cannot interact with neutrons directly due to the charge neutrality of neutrons. Nevertheless, these excitations can influence the lattice dynamics, especially when both are in the same frequency range.

Based on a quantitative analysis of an excitonic-like model for the IV state [54], it can be elaborated that the presence of sufficiently 'soft' excitations related to a redistribution of the electron density affects the lattice dynamics via two separated channels.

First, it is a renormalization of the frequencies of 'normal' phonons (which are phonons typical for the actual structure and substance). In fact, with the 'breathing' or 'full-symmetric' mode of charge density distortions for a finite-radius exciton formed by a loosely bound f-electron taken into account, it becomes possible to describe 'dips' or 'kinks' in the dispersion curves of LA phonons in both the [110] and [111] directions (see Fig. 9, Fig. 15). The electron dipole charge-density-distortion mode also takes part in phonon renormalization, suggested to be responsible for the general softening of phonon frequencies.

Second, it is the production of 'excess' vibrones, not implied by the symmetry of crystal latticed modes. This effect is a direct consequence of the so-called resonant violation of the adiabatic approximation. Usually, in analyzing the lattice dynamics of solids, the adiabatic approximation is presumed to hold for the electron subsystem. In the case of Sm-based systems, considered as carriers of the IV state, the adiabatic approximation is violated by the presence in the electronic spectrum of low-frequency modes ($E_{ex} \approx 10-20$ meV) corresponding to charge transfer excitations in the spectrum of mixed wave function (6). A situation is possible where $\hbar\omega_{max} \geqslant E_{ex}$, with $\omega_{max}$ being the maximum observable frequency of phonons. For such electron modes, a crystal lattice already appears to be not stationary, and mixed vibronic states can develop, being provided by the dynamic Jahn–Teller effect, i.e., by a transformation of the vibrational potential under the influence of hybridizing electron states. As a result, 'additional' modes (see Fig. 15) appear, with the particular properties determined by the character of the electron charge distribution for this excitation in the spectrum of new wave function (6) and features of inter-ionic interaction. Detailed consideration of the particular case of SmS and $SmB_6$ is given in the original study [54].

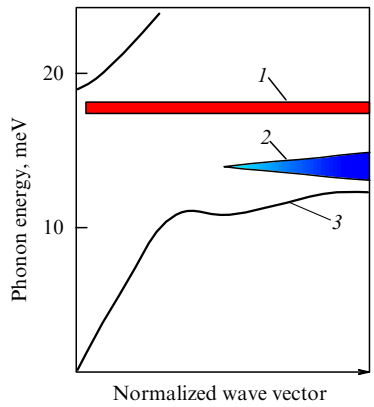


**Figure 15.** Schematic picture presenting 'extra'-phonon modes observed in an $SmB_6$ single crystal by inelastic neutron scattering [14]. *1* — nonadiabatic 'local' mode ($\omega_e < \omega_{ph}$), *2* — nonadiabatic 'coherent' mode ($\omega_e < \omega_{ph}$), *3* — deformation of the acoustic longitudinal mode due to the presence of charge fluctuations.

From the formal standpoint, local fluctuations of valence can be presented as some defect of force constants in the atomic vibration subsystem. If the difference between electron density distributions for ground and excited vibronic states corresponding to the mixture of electron and lattice degrees of freedom is large, this defect is well localized. This localization of the 'defect' results in the appearance of a dispersionless and nonpolarized local or quasilocal mode. If this difference is small, then the degree of localization of the 'defect' is low, and there is coherent excitation that is able to propagate in the crystal lattice almost like an ordinary phonon.

The above consideration corresponds well with experimental findings, as shown in Fig. 15. Vibrations of these two types, which can appear as a result of the interaction of a soft deformation mode and low-frequency lattice vibrations [54], [4] are just observed in $SmB_6$, as a dispersionless mode and a satellite one related to the longitudinal acoustic phonon. The satellite mode exists only at a sufficiently low temperature,

[4] In [54], applying the full-symmetric mode of charge density deformation to the hierarchy of force constants peculiar to $SmB_6$ results in a latticed defect of the dipole symmetry. It interacts with optical and acoustic phonons at the specified values of wavevectors q in the Brillouin zone.

because the increase in temperature results in changing the characteristics of screening and reduces the energy difference between two weakly deformed states.

A similar physical picture also holds for SmS. There is a dispersionless mode observed experimentally [49], but a coherent vibron has not been observed, perhaps due to strong damping, resulting in a large energy width of longitudinal phonons.

It is possible to describe this problem using a somewhat different 'language'.

A basic feature of the IV state is the presence of very soft full-symmetric ($\Gamma_1$) electronic excitations. Due to this feature of the electron subsystem, a violation (of a resonant character) of the adiabatic approach traditional for consideration of lattice dynamics (with $\omega_{el} \gg \omega_{ph}$) occurs. This situation may result in the appearance of additional vibrational modes, because the effective 'dimensionality' for the degrees of freedom for atomic movements in the crystal increases. The characteristics of these additional modes are determined by the relation between $\omega_{el}$ and $\omega_{ph}$ for particular phonon modes with energies close to $\omega_{el}$ (Fig. 15).

When $\omega_{el} < \omega_{ph}$ (which may be the case for optical phonons), some kind of static defect of force constants is realized (the phonon frequency is higher than that of the electronic exciton, and everything (polarization, anisotropy) is averaged). Consequently, there is no dispersion or polarization for the corresponding extra vibration mode. An electron excitation at $\omega_{el}$ is an excitation with charge transfer, but without a change in symmetry in our particular case of the $SmB_6$ spectrum of an intermediate-radius exciton. Under the conditions of a strong hierarchy of interactions in $SmB_6$, the energy position of the local mode specific to this defect is attached to the energy (at $q \approx 0$) of the optical phonon that is the nearest in energy to $\omega_{el}$ (a lower optical phonon). This local mode (see Fig. 9), naturally, does not have polarization, and disappears as the temperature decreases, i.e., when depopulation of the excited excitonic state becomes considerable.

Another form of the manifestation of nonadiabaticity is related to the case $\omega_{el} \geqslant \omega_{ph}$, which occurs for acoustic phonons. This means that electron and phonon excitations can be in phase (there is a mixed state similar to the one specific to the dynamic Jahn–Teller effect due to the full-symmetric electron excitation mode). We can say that the phonon appears as a result of the transition between two electron states, and is therefore a dynamical 'coherent defect'. With an increase in temperature, the potentials of these states come to symmetric positions, and the energy of the corresponding phonon excitation reduces to zero. The intensity of such excitation is maximal at wave vectors where the frequencies ($\omega_{el}$ and $\omega_{ph}$) are closest to one another, i.e., close to the boundary of the Brillouin zone (for instance, at the $\Gamma$ point, the degree of nonadiabaticity $\omega_{ph}/\omega_{el}$ is near 0!).

To summarize the discussion of specific manifestations of the electron–phonon coupling for IV Sm-based systems, we can formulate the following general concept.

Both cases $\omega_{el} < \omega_{ph}$ and $\omega_{el} > \omega_{ph}$ can be represented as extreme variants of the existence of an exciton polaron in the crystal lattice (the exciton producing a polarization of the crystal lattice near its location), which results in a deformation of the potential profile for atomic vibrations of the 'cluster' formed by atoms located close to the exciton. The formation of the extra ('local' and 'coherent') vibrational modes results from the interaction of electron excitations corresponding to the electron density deformation with optical and acoustic (longitudinal) modes.

An intermediate-radius exciton is itself responsible for renormalization of the 'normal' adiabatic phonon spectrum [14, 54–57]. The finite size of the exciton determines the shape of its form factor in the momentum space. The form factor of the exciton affects the strength of the renormalization of phonons. The form factor has a maximum at some intermediate value of the reduced wave vector, which determines the position of the maxima of renormalization effects approximately halfway between the center and the zone boundary. That is just the location of 'kinks' on LA phonon dispersion curves observed experimentally.

For completeness, the temperature effects observed for $SmB_6$ should be mentioned. They are strong enough (up to 15% at zone boundary) for the [100] and [111] directions (see Fig. 12 and Fig. 1 in Ref. [16]) and are not observed for $LaB_6$ or $PrB_6$.

One possible reason for these effects in $SmB_6$ could be a strong renormalization of the $q$-dependence (including specific anisotropy selective for the [100] and [111] directions) and the energy structure of the f-electron excitation spectra [59] that occurs near the boundary of the first Brillouin zone for the above symmetry directions at temperatures in the range 50–100 K. The strong influence of the electron subsystem on acoustic phonons with wave vectors in the range of the second half of the Brillouin zone is directly confirmed by a recent study of the RE vibration contribution to the acoustic branch of $DyB_6$ [63] and $GdB_6$ [64] using X-ray inelastic scattering. It shows a strong renormalization of the phonon energy as a result of replacement of the RE element (the relative change in the energy exceeds the relative difference of masses between Gd and Dy fourfold) and, moreover, as a result of temperature variation in the vicinity of the magnetic long-range ordering transition. In fact, the energy of the flat part of the acoustic phonon dispersion curve at room temperature for $DyB_6$ is located at about 7 meV, to be compared with 8 meV for $GdB_6$, 11 meV for $SmB_6$ and $PrB_6$ (see Fig. 9 and Fig. 12), and 13 meV for $LaB_6$.

Of course, these observations require a special theoretical analysis; unfortunately, the well-known theoretical approaches to the phonon description in the vicinity of a phase transition [65] seem not to be directly suitable in the present case. Nevertheless, the developed technique may be regarded as one of the useful tools.

In summary, we can conclude that the electron–phonon interaction in the range of acoustic phonon energies is quite strong for compounds of this type.

### 4.2 $REB_{12}$

The lattice dynamics of $REB_{12}$ are quite similar to those of $REB_6$ in general. Of course, there is a difference in the number of phonon modes, the value of the boundary phonon energy, and the energy of the flat part of the acoustic branch determining the position of the first peak in the PDOS: the latter is approximately 1.5 times higher in $REB_{12}$ (cf. Fig. 5 and Fig. 6). $REB_{12}$-type systems exist as stable compounds only for several heavy RE ions, and there is no evidence of the strong f-electron instability for any of them. Nevertheless, $MB_{12}$ compounds exist for $M$ being a transition element like Zr or Y. Therefore, it is possible to observe the influence of the d-element substitution on the low-energy part of the vibration spectrum.

We have studied the phonon modes in the $ZrB_{12}$ single crystal [22, 23]. This substance is interesting due to the highest temperatures of any superconducting transition (after $MgB_2$) ($T_c \approx 6$ K) among rich borides.

It was previously suggested in [66] that the superconductivity in $YB_6$ and $ZrB_{12}$ is directly connected with vibrations of boron complexes. On the other hand, the much smaller isotope effect on $T_c$ produced by boron than by Zr in $ZrB_{12}$ suggests that lattice vibration modes involving Zr atoms play a key role in the electron–phonon coupling responsible for superconductivity [67, 68].

We have performed *ab initio* calculations, as well as detailed single-crystal INS measurements of the lattice dynamics in this compound. Experimental results have also been used for fitting the phenomenological forced-constant model (using the UNISOFT code [46]).

It is seen from *ab initio* calculations that, similarly to RE dodecaborides, the phonon spectrum in $ZrB_{12}$ is mainly determined by the boron sublattice vibrations, and extends up to energies $\sim 140$ meV (see Fig. 16). Although the *ab initio* calculations do not yield a quantitative description of acoustic phonon dispersion, they do provide important information on the lattice dynamics of $MB_{12}$ compounds in general. The phenomenological model results in a much better description of acoustic modes [cf. Fig. 17 (*ab intio*) and Fig. 18 (phenomenological)].

The low-energy region has a peculiar structure with large weakly dispersive parts in the acoustic phonon branches and a gap between the acoustic and optical branches. Such a shape of the vibration spectrum can be understood in terms of the hierarchy of interatomic interactions. In analogy with $REB_6$ and $REB_{12}$, the Zr ions are loosely bound within the rigid boron network, and their vibrations therefore have a quasilocal character. The energy of these quasilocal Zr vibration modes was determined to be approximately 17.5 meV ($q = q_{max}$), which is a relatively low value with respect to simple scaling due to the ratio of atomic masses based on the Einstein model ($\sim 21$ meV). Thus, the essential role of the electronic contribution to the formation of the force potential for atomic vibration is demonstrated experimentally in rich borides.

The results of both *ab initio* calculations and INS measurements further indicate that the Zr vibration modes make an appreciable contribution to electron–phonon interactions and may therefore take part in the formation of the superconducting state with a rather high transition temperature $T_c = 6$ K.

We return to strongly correlated compounds and consider $YbB_{12}$, a representative of the so-called Kondo semiconductors [69], systems that demonstrate a correlated transition between Kondo-metal behavior at relatively high temperatures and the low-temperature nonmagnetic state with a narrow gap in the electron density of states at the Fermi energy [70–72]. This transition is accompanied by an extremely strong transformation of the magnetic excitation spectrum, in particular, a spin gap of the order of 200 K is developed during this transition in a narrow temperature range around 50 K [37, 73, 74]. On the other hand, almost no difference has been observed between phonon energies of $YbB_{12}$ and its nearest neighboring compound without a magnetic moment, $LuB_{12}$, in a wide temperature range.

From the standpoint of features of the electron–phonon interaction in strongly correlated systems, it is interesting to

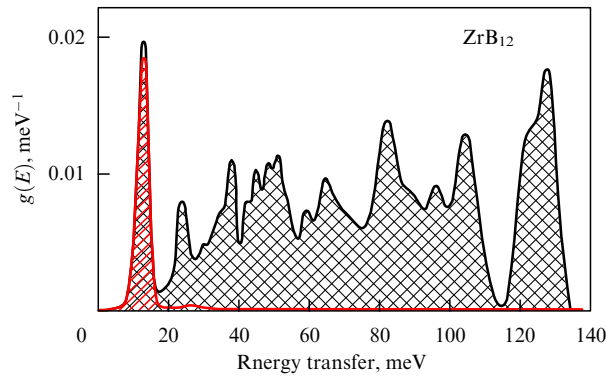


**Figure 16.** PDOS of $ZrB_{12}$ calculated in [23] convoluted with the same resolution function as in Fig. 11. Cross-hatched area: total PDOS; hatched area (in red color): partial zirconium PDOS.

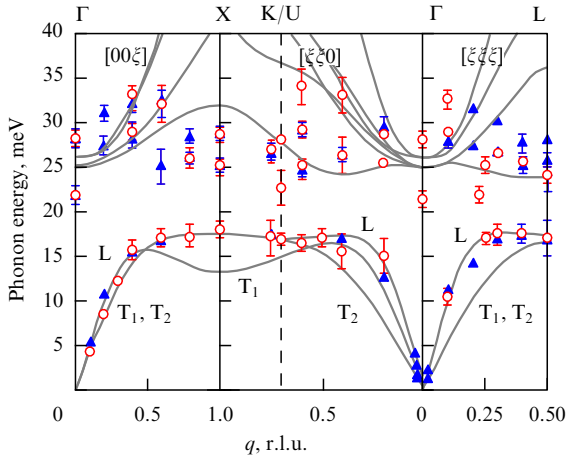


**Figure 17.** Phonon dispersion in $ZrB_{12}$ measured along the principal symmetry directions [23, 22]. Lines: *ab initio* calculation. L and $T_1$, $T_2$ denote the longitudinal- and transverse-acoustic branches, with $T_1$ having its polarization vectors within the experimental scattering plane and $T_2$ perpendicular to this plane. Symbols: circles and triangles correspond to branches measured in the respective longitudinal and transverse ($T_1$) configurations.

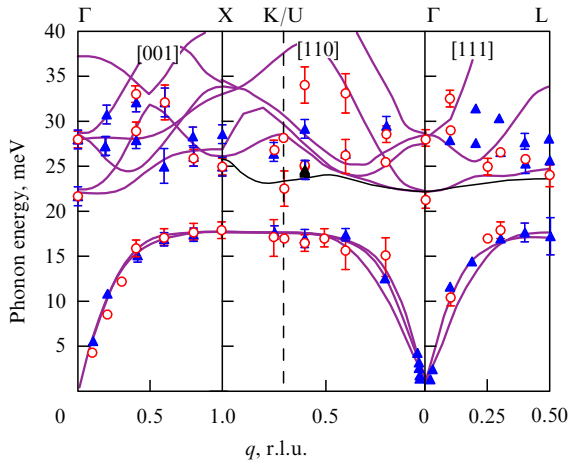


**Figure 18.** Low-energy phonon dispersion in $ZrB_{12}$. Symbols: experiment as in Fig. 17. Lines: force-constant calculation derived from the model similar to the one in Ref. [18] for $LuB_{12}$ by taking the difference in atomic masses into account and adjusting the Zr–Zr and Zr–B interactions.

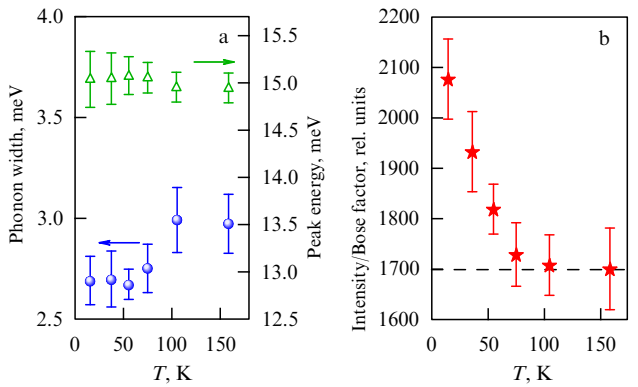


**Figure 19.** Parameters of the low-energy phonon peak in the $YbB_{12}$ spectrum as a function of temperature: (a) phonon peak width (circles) and energy (triangles), (b) intensity corrected by the standard Bose factor for a 13.5 meV phonon: experimental data (stars); dashed line — behavior of the phonon intensity obtained from data at 150 K according to the normal Debye–Waller factor (defined by the PDOS). (Reproduced from [45].)

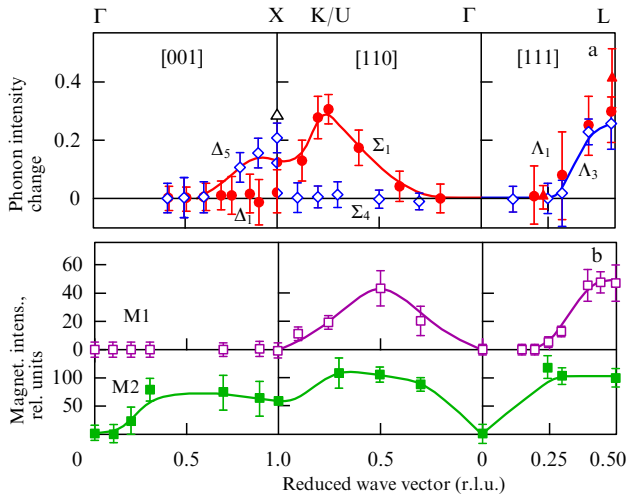


**Figure 20.** (a) Relative temperature change between 80 K and 10 K $(\mathrm{Int}_{10}-\mathrm{Int}_{80})/\mathrm{Int}_{80}$ of the integrated intensities of acoustic phonon excitations along the principal symmetry directions in $YbB_{12}$: $\Delta_1$ (LA) and $\Delta_5$ (TA) along [001], $\Sigma_1$ (LA) and $\Sigma_4$ (TA) along [110], $\Lambda_1$ (LA) and $\Lambda_3$ (TA) along [111]. Filled and open symbols respectively denote longitudinal (LA) and transverse (TA) modes. (b) Integrated intensities of the low-energy magnetic excitations M1 (open squares) and M2 (filled squares) in the Kondo insulator regime at $T = 5$ K for reduced q vectors along the principal symmetry directions. (Plot taken from [20].)

analyze a possible relation of the joint metal–insulator and magnetic–nonmagnetic transition to the features of lattice dynamics of $YbB_{12}$. In this system, as was already noted [73, 75], the magnetic modes overlap with some phonon ones in the energy range 15–20 meV (see the PDOS in Fig. 10) near the gap edge in magnetic excitation spectra. This fact gives rise to an assumption of interaction between them and even to ideas about a certain role [76] of the lattice dynamics in the formation of conditions for the sharp transformation of the magnetic excitation spectrum from spin-fluctuation to gap-like, which looks similar to some kind of phase transition with a 'hidden parameter'.

The first evidence of the presence of a possible connection between phonons and the rearrangement of the magnetic spectrum was found by analyzing the temperature dependence of parameters of the first peak (at about 15 meV) in the PDOS spectrum of $YbB_{12}$, as a function of temperature [45], shown in Fig. 19. Experiments have been done by the TOF technique with the initial energy of neutrons 80 meV. A noticeable increase ($\approx 25\%$) in the intensity of the phonon peak (see Fig. 19b) was observed in [45] in the temperature range of gap formation in magnetic excitation spectra, as well as in the charge density of states near the Fermi energy. It was observed under the conditions (a sufficiently high value $Q \geqslant 10$ Å$^{-1} = 100$ nm$^{-1}$) when a direct magnetic contribution of f-electrons to the intensity of inelastic neutron scattering did not exceed a few percent of the intensity value of the phonon-originating component. Interestingly, in the same temperature range of the electronic gap formation, the variation of the phonon peak width in the PDOS was also fixed (see Fig. 19a), which looks like another manifestation of the electron–phonon interaction.

Further research connected with this mysterious observation is being carried out by the TAS technique using single crystals of $YbB_{12}$ [20] and based on the symmetry analysis given in [45]. Measurements of the phonon parameters were performed at two temperatures, 80 K and 10 K, which are in correspondence with two regimes of the electron subsystem: spin-fluctuation ('high-T') and gap-like ('low-T') for the magnetic excitation spectrum. The energy and intensity of a number of phonon modes were analyzed in the energy range 0 – 30 meV. Significant changes in energy have not been discovered; however, the intensities of some longitudinal and transverse phonons have demonstrated a substantial deviation from the temperature behavior normally determined by a Bose factor. There was a 15–30% increase in intensity for some acoustic branches [20], with the wave vector close to the Brillouin zone boundary corresponding to a phonon energy of about 15 meV, which is consistent with earlier data for measurements of polycrystalline samples on a TOF spectrometer [45]. An effect of the intensity increase (see Fig. 20) was observed for those branches whose symmetry allowed interaction with magnetic dipole excitations, and in that area of wave vectors where dispersive low-temperature magnetic modes denoted as M2 and M1 in [75] (20 meV and 15 meV, respectively) are present in the magnetic spectrum at low temperatures.

The features observed obviously indicate a manifestation of some kind of magneto-vibrational interaction. A quite unusual effect is the presence of a strong renormalization of intensity, but not a renormalization of phonon energies. The microscopic reasons for such a behavior could be related to the strong hierarchy of forces of inter-atomic interactions obtained from analyses of phonon dispersion. This corresponds to the picture where the formation of the acoustic mode is determined by vibrations of loosely coupled heavy ions, located in a 24-boron cage, and the other 36 optical branches are related to the boron hard framework with the RE–B and B–B interactions. Under the conditions of high crystalline symmetry and a large number of atoms in the primitive cell, a large number of vibration modes appear to be symmetry-connected, which is exactly the case for $REB_{12}$. It is possible that their interplay with each other results in a specific manifestation of the inter-subsystem (in the present case, magneto-vibrational) interaction. A renormalization of polarization vectors [5] is observed instead of the renormaliza-

[5] Its modulus just defines the atomic displacement amplitude in a given mode, which is related to the intensity [see Eqns (3)–(5)] of the signal at a particular energy in the neutron scattering spectrum.

tion of phonon energies. We note that such a type of effect has been observed in HTSC phonon studies [77, 78] in the range of temperatures corresponding to the superconducting transition with the electron energy gap formation. In the discussion, it was related by the authors to the specifics of the electron–phonon interaction under a special condition just applied for $YbB_{12}$ (high symmetry and a large number of atoms).

It is possible that the observed interaction is evidence of a certain role of the lattice subsystem in the sharp change of the regime of the magnetic subsystem (spin-fluctuation to gap-like) in a narrow temperature range around 50 K. Additional evidence for this transformation scenario is provided by recent results of a study of excitation spectra of $Yb_{0.8}Zr_{0.2}B_{12}$ [79, 80] by inelastic neutron scattering. It was established in that study that strong damping of the sharp transition for the magnetic spectrum and suppression of the anomalous temperature dependence of a 15 meV peak in the phonon spectrum are simultaneously observed due to substituting a small part of Yb atoms by Zr, which is different from Yb not only in the atomic mass but also in the number of valence electrons and the d-band type (4d instead of 5d) close to the Fermi energy. Both factors are important for atomic dynamics, and, consequently, it can be assumed that atomic dynamics play a substantial role in the formation of the ground state of the $YbB_{12}$ system.

## 5. Conclusion

An extended experimental study of the phonon spectra of $MB_6$ and $MB_{12}$ has provided quantitative characteristics of the spectral features, details of the energy structure, and the dispersion relation. The first parameters allow making a comparison within a variety of boron-based materials and obtaining evidence of the similarity of boron- and graphite-based materials. The details of experimental observations and model calculations for phonon dispersion provide a better understanding of the limitations of different model considerations of dynamics related to the influence of specific features of lattice dynamics on thermodynamic properties.

In particular, the clear nonmonotonic T-dependence of specific heat in the low-temperature region (between 15 and 30 K) observed for dodecaborides [81] with respect to hexaborides appears to originate from a considerable increase in the energy of the flat part of the acoustic mode dispersion in dodecaborides with respect to hexaborides. The importance of taking the features of low-energy lattice dynamics into account for understanding the thermal expansion temperature behavior in strongly correlated semiconductors $SmB_6$ and $YbB_{12}$ has been clearly demonstrated in the analysis done in [82].

Some general conclusions following from the results presented here are as follows.

The dynamics of crystalline lattices for $MB_6$ and $MB_{12}$ have many common features. Physically, this observation very likely results from similarities in the hierarchy of interatomic interactions in these classes of systems, which are characterized by a hard three-dimensional boron-cage framework with voids occupied by metallic ions. The band gap structure of phonon spectra is a quite interesting peculiarity. Systems with such a phonon band gap have recently been discussed from the standpoint of the possibility of realizing control over sound and even heat flow (in the THz range of phonons, just as in borides) [83].

For a correct description of low-energy lattice dynamics, the contribution of electronic correlations and the immediate contribution of d- and f- electrons originating from $M$-type atom must be taken into account in the resulting dynamical-force matrix.

The electron–phonon interaction is determined to a substantial degree by the specifics of unfilled electronic shells (strong electronic correlations, spin fluctuations, intermediate valence). An important factor is therefore the resonant character of interaction between electronic, lattice, and magnetic subsystems, which results, in particular, in a resonant violation of the adiabatic approximation in intermediate-valence systems. Experimental observation of these effects appears to be an important experimental finding.

The final remarks concern the basic similarity between boron and carbon materials, pointed out at the beginning of this paper. The presented data on lattice dynamics show that these materials have a common structure of atomic vibration spectra; the specifics of these spectra are preserved in general for binary (boron-based) compounds and their (carbon-based) structural modifications. Recent theoretical and experimental studies clearly show the prospects of boron-based materials, which could be obtained in a quasi-two-dimensional shape [84, 85], like graphene, 3-D-like carbon buckyballs [41], or nanotubes from boron nitride (BNNT) compounds [86] having quite promising electronic (2D), mechanic, thermal, and chemical (BNNT) properties.

In conclusion, we mention that the study of phonons demonstrates a very important interplay between lattice and electronic excitation spectra in strongly correlated electron systems. Neutrons provide a unique opportunity to study both sides simultaneously, as was mentioned above for the cases of $SmB_6$ and $YbB_{12}$. The growing interest in so-called 'topological insulators', in particular, $SmB_6$ as a representative [87, 88] of this branch of physics related to strongly correlated electron systems, may be the reason for a more detailed and specially focused analysis of the existing and newly obtained experimental data from the standpoint of the interplay between magnetic, electron, and phonon subsystems. A large amount of information in this adjoining field of neutron spectroscopy oriented toward magnetic excitation in strongly correlated electron systems has been collected so far. This would be the topic of a separate review.

**Acknowledgements**

The author express gratitude to colleagues without whom this work would have been impossible: N Yu Shitsevalova, V B Filipov, I P Sadikov, V N Lazukov, J-M Mignot, A S Ivanov, P P Parshin, R I Buwely, and K S Nemkovski; the fruitful discussions with Yu M Kagan, K A Kikoin, A S Mishchenko, and V G Orlov are highly appreciated. Memorable brainstorming discussions with Yu B Paderno are the source of inspiration for the future.

The hospitality and local support of ILL (Grenoble), LLB (CNRS-CEA, Saclay), and ISIS (Didcot) are invaluable. Special gratitude is offered to N V Znamenskiy and A P Menushenkov for the support and interest in the project.

The present study was partially (parts 1, 2, 4) supported by the Russian Science Foundation, Grant No. 14-22-00098.

## References


1. Mori T, in *Handbook on the Physics and Chemistry of Rare Earths* Vol. 38 (Eds K A Gschneidner (Jr.), J-C Bunzli, V Pecharsky) (Amsterdam: North-Holland, 2008) p. 105
2. Mori T *Boron Rich Solids*: *Sensors, Ultra High Temperature Ceramics, Thermoelectrics, Armor* (NATO Science for Peace and Security Series, Ser. B, Eds N Orlovskaya, M Lugovy) (Dordrecht: Springer, 2011)
3. Vainshtein É E, Blokhin S M, Paderno Yu B *Sov. Phys. Solid State* **6** 2318 (1965); *Fiz. Tverd. Tela* **6** 2909 (1964)
4. Werheit H et al. *J. Phys. Condens. Matter* **23** 065403 (2011)
5. Greenwood N N, Parish R V, Thornton P *Q. Rev. Chem. Soc.* **20** 441 (1966); Hoard J L, Hughes R E "Elementary boron and compounds of high boron content: structure, properties, and polymorphism", in *The Chemistry of Boron and Its Compounds* (Comp. E L Muetterties) (New York: Wiley, 1967) Ch. 2, pp. 25 – 154
6. Batlogg B, Schmidt P H, Rowell J M, in *Valence Fluctuations in Solids* (Eds L M Falicov, W Hanke, M B Maple) (Amsterdam: North-Holland, 1981) p. 267
7. Kasaya M et al. *J. Magn. Magn. Mater.* **47 – 48** 429 (1985)
8. Ishii M et al. *Solid State Commun.* **20** 437 (1976)
9. Mörke I, Dvorák V, Wachter P *Solid State Commun.* **40** 331 (1981)
10. Zirngiebl E et al. *J. Magn. Magn. Mater.* **54 – 57** 359 (1986)
11. Smith H G et al. *Solid State Commun.* **53** 15 (1985)
12. Schell G et al. *Phys. Rev. B* **25** 1589 (1982)
13. Compf F, Progress Report Teilinstitut Nukleare Festkörperphysik 1.6.1977 – 31.5.1978. KfK 2670 (Ed. K Käfer) (Karlsruhe: Kernforschungszentrum, 1978) p. 17; http://bibliothek.fzk.de/zb/kfk-berichte/KFK2670.pdf
14. Alekseev P A et al. *Europhys. Lett.* **10** 457 (1989)
15. Alekseev P A et al. *Physica B* **180 – 181** 281 (1992)
16. Mignot J-M, Alekseev P A *Physica B* **215** 99 (1995)
17. Nemkovski K S, Alekseev P A, Mignot J-M, Tiden N N *Phys. Status Solidi C* **1** 3093 (2004)
18. Nemkovski K S et al. *J. Solid State Chem.* **179** 2895 (2006)
19. Rybina A V et al. *Crystallogr. Rep.* **52** 770 (2007); *Kristallogr.* **52** 800 (2007)
20. Alekseev P A et al. *J. Phys. Condens. Matter* **24** 205601 (2012)
21. Alekseev P A et al. *Phys. Solid State* **52** 914 (2010); *Fiz. Tverd. Tela* **52** 858 (2010)
22. Rybina A V et al. *Phys. Solid State* **52** 894 (2010); *Fiz. Tverd. Tela* **52** 842 (2010)
23. Rybina A V et al. *Phys. Rev. B* **82** 024302 (2010)
24. Gurevich I I, Tarasov L T *Low-Energy Neutron Physics* (Amsterdam: North-Holland Publ. Co., 1968); Translated from Russian: *Fizika Neitronov Nizkikh Energii* (Moscow: Nauka, 1965)
25. Sköld K, Price D L (Eds) *Neutron Scattering* (Methods in Experimental Physics, Vol. 23, Pt. C, Eds-in-Chief R Celotta, J Levine) (Amsterdam: Elsevier, 1987)
26. *The ILL Yellow Book*, ILL (Grenoble: Institut Laue-Langevin, 2008); https://www.ill.eu/fr/instruments-support/instruments-groups/yellowbook/
27. MARI spectrometer , http://www.isis.stfc.ac.uk/instruments/mari
28. Dorner B *Coherent Inelastic Neutron Scattering in Lattice Dynamics* (Berlin: Springer-Verlag, 1982)
29. Shirane G, Shapiro S M, Tranquada J M *Neutron Scattering with a Triple-Axis Spectrometers*: *Basic Techniques* (New York: Cambridge Univ. Press, 2004)
30. Kagan Yu *Sov. Phys. JETP* **15** 954 (1962); *Zh. Eksp. Teor. Fiz.* **42** 1375 (1962)
31. Parshin P P, Zemlyanov M G, Soldatov P I *JETP* **74** 400 (1992); *Zh. Eksp. Teor. Fiz.* **101** 750 (1992)
32. Parshin P P et al. *JETP Lett.* **51** 434 (1990); *Pis'ma Zh. Eksp. Teor. Fiz.* **51** 380 (1990)
33. Zemlyanov M G et al. *JETP* **77** 148 (1993); *Zh. Eksp. Teor. Fiz.* **104** 2538 (1993)
34. Parshin P P et al. *Appl. Phys. A* **74** 1657 (2002)
35. Parshin P P, Zemlyanov M G, Brand R A *Crystallogr. Rep.* **52** 1020 (2007); *Kristallogr.* **52** 1057 (2007)
36. Alekseev P A et al. *JETP* **81** 586 (1995); *Zh. Eksp. Teor. Fiz.* **108** 1064 (1995)
37. Nefeodova E V et al. *Phys. Rev. B* **60** 13507 (1999)
38. Weber W, Thorpe M F *J. Phys. Chem. Solids* **36** 967 (1975)
39. Richter W, Hausen A, Binnenbruck H *Phys. Status Solidi B* **51** 115 (1972)
40. Rols S et al. *Phys. Rev. Lett.* **85** 5222 (2000)
41. Zhai H-J et al. *Nature Chem.* **6** 727 (2014)
42. Cappelletti R L et al. *Phys. Rev. Lett.* **66** 3261 (1991)
43. Pintschovius L et al. *Phys. Rev. Lett.* **69** 2662 (1992)
44. Smith H G et al. *Solid State Commun.* **53** 15 (1985)
45. Rybina A V et al. *J. Phys. Conf. Ser.* **92** 012074 (2007)
46. Elter P, Eckold G *Physica B* **276 – 278** 268 (2000)
47. Loewenhaupt M, Fischer K H, in *Handbook on the Physics and Chemistry of Rare Earths* Vol. 16 (Eds K A Gschneidner (Jr.), L Eyring) (Amsterdam: North-Holland, 1993) p. 1
48. "Challenges in Plutonium Science" *Los Alamos Science* (26) (2000)
49. Mook H A et al. *Phys. Rev. B* **18** 2925 (1978)
50. Mook H A, McWhan D B, Holtzberg F *Phys. Rev. B* **25** 4321(R) (1982)
51. Alekseev P A et al. *Phys. Rev. B* **74** 035114 (2006)
52. Stusser N et al., in *Valence Instabilities*: *Proc. of the Intern. Conf, Zürich, Switzerland, April 13 – 16, 1982* (Eds P Wachter, H Boppart) (Amsterdam: North-Holland, 1982) p. 69
53. Alekseev P A *Physica B* **186 – 188** 365 (1993)
54. Kikoin K A, Mishchenko A S *JETP* **77** 828 (1993); *Zh. Eksp. Teor. Fiz.* **104** 3810 (1993)
55. Mishchenko A S, Kikoin K A *J. Phys. Condens. Matter* **3** 5937 (1991)
56. Kikoin K A *JETP* **58** 582 (1983); *Zh. Eksp. Teor. Fiz.* **85** 1000 (1983)
57. Stevens K W H *J. Phys. C Solid State Phys.* **9** 1417 (1976)
58. Kikoin K A, Mishchenko A S *J. Phys. Condens. Matter* **7** 307 (1995)
59. Alekseev P A et al. *J. Phys. Condens. Matter* **7** 289 (1995)
60. Holland-Moritz E, Zirngiebl E, Blumenröder S *Z. Phys. B* **70** 395 (1988)
61. Alekseev P A et al. *Phys. Rev. B* **65** 153201 (2002)
62. Alekseev P A et al. *JETP* **111** 285 (2010); *Zh. Eksp. Teor. Fiz.* **138** 321 (2010)
63. Iwasa K et al. *J. Phys. Soc. Jpn.* **81** 113601 (2012)
64. Iwasa K et al. *Phys. Rev. B* **84** 214308 (2011)
65. Aksenov V L, Plakida N M, Stamenković S *Neutron Scattering by Ferroelectrics* (Singapore: World Scientific, 1990); Translated from Russian: *Rasseyanie Neitronov Segnetoelektrikami* (Ed. N M Plakida) (Moscow: Energoatomizdat, 1984)
66. Fisk Z *AIP Conf. Proc.* **231** 155 (1991)
67. Chu C W, Hill H H *Science* **159** 1227 (1968)
68. Fisk Z et al. *Phys. Lett. A* **37** 251 (1971)
69. Riseborough P S *Adv. Phys.* **49** 257 (2000)
70. Iga F, Kasaya M, Kasuya T *J. Magn. Magn. Mater.* **76 – 77** 156 (1988)
71. Takabatake T et al. *J. Magn. Magn. Mater.* **177 – 181** 277 (1998)
72. Okamura H et al. *J. Phys. Soc. Jpn.* **74** 1954 (2005)
73. Bouvet A et al. *J. Phys. Condens. Matter* **10** 5667 (1998)
74. Alekseev P A et al. *J. Phys. Condens. Matter* **16** 2631 (2004)
75. Nemkovski K S et al. *Phys. Rev. Lett.* **99** 137204 (2007)
76. Sluchanko N E et al. *JETP* **113** 468 (2011); *Zh. Eksp. Teor. Fiz.* **140** 536 (2011)
77. Reznik D et al. *Phys. Rev. B* **78** 094507 (2008)
78. De Filippis G et al. *Europhys. Lett.* **91** 47007 (2010)
79. Alekseev P A et al. *Solid State Sci.* **14** 1584 (2012)
80. Nemkovski K S et al. *Phys. Rev. B* **81** 125108 (2010)
81. Takegahara K, Kasuya T *Solid State Commun.* **53** 21 (1985)
82. Nefedova E V, Alekseev P A, Lazukov V N, Sadikov I P *JETP* **96** 1113 (2003); *Zh. Eksp. Teor. Fiz.* **123** 1266 (2003)
83. Maldovan M *Nature* **503** 209 (2013)
84. Penev E S et al. *Nano Lett.* **12** 2441 (2012)
85. Zhou X-F et al. *Phys. Rev. Lett.* **112** 085502 (2014)
86. Sakhavand N, Shahsavari R *J. Phys. Chem. C* **118** 22730 (2014)
87. Dzero M et al. *Phys. Rev. Lett.* **104** 106408 (2010)
88. Legner M, Rüegg A, Sigrist M *Phys. Rev. B* **89** 085110 (2014)